Disruption of Canonical TGF-β/SMAD Signaling Pathway by TSCA High-Priority Phthalate Plasticizers: A Dual-Engine Molecular Docking Analysis

Mrinmoy Mandal[1,†], Naveen Kumar[2,†,*], Pooja Kadyan[3], Sapna Redhu[4], Jayendra Kumar Singh[5], Kaushalendra[6], Nisha Yadav[1], Divya Tyagi[1], Vikrant[7] and Varsha Singh[8]

[1]*Department of Chemistry, School of Basic & Applied Science, Sanskaram University, Patauda-124108, Jhajjar, Haryana, India*

[2]*Department of Zoology, School of Basic & Applied Science, Sanskaram University, Patauda-124108, Jhajjar, Haryana, India*

[3]*Department of Zoology, Sant Shiromani Shri Sain Bhagat Government College, Jind (126102), Haryana, India*

[4]*Department of Biotechnology, Chaudhary Devi Lal University, Sirsa-125055, India*

[5]*School of Business, University of Petroleum and Energy Studies, Dehradun-248007, Uttarakhand, India*

[6]*Department of Zoology, Pachhunga University College Campus, Mizoram University, Aizawl - 796001, India*

[7]*Department of Botany, School of Basic & Applied Science, Sanskaram University, Patauda-124108, Jhajjar, Haryana, India*

[8]*Department of Zoology, Institute of Science, Banaras Hindu University (BHU), Varanasi, 221005, Uttar Pradesh, India*

Abstract: Uses of Plastic have increased worldwide and phthalate esters - released continuously from plastic matrices due to their non-covalent bonding - are among the most abundantly detected chemical additives in human biomonitoring globally. Seven phthalates are currently designated as High-Priority Substances under active federal risk evaluation by the US EPA under Toxic Substances Control Act (TSCA). Of these, five - di(2-ethylhexyl) phthalate (DEHP), di-n-butyl phthalate (DBP), diisobutyl phthalate (DIBP), benzyl butyl phthalate (BBP), and dicyclohexyl phthalate (DCP) - were selected based on dominance in environmental detection and biomonitoring data. Despite growing evidence linking phthalates to various diseases, no study has evaluated all five together against a complete signaling pathway spanning membrane, cytoplasmic, and nuclear protein targets. Therefore, dual-engine molecular docking was performed using AutoDock 4 and AutoDock Vina against four resolved TGF-β/SMAD signaling Pathway targets - TGFβRI (3TZM), TGFβRII (5E92), SMAD2 (1DEV), and SMAD3/SMAD4 (1U7F) - the only pathway among 18 studied which have all three cellular compartments. All five showed binding above −6.0 kcal mol^{-1} at TGFβRI, TGFβRII, and SMAD3/SMAD4 in both engines. Affinity hierarchy was consistent - DCP > BBP > DIBP > DBP > DEHP - across all four targets. At SMAD2, only DCP showed stable binding and remaining four produced no stable/convergent docking pose under the specified conditions. DCP is the least detected yet showed strongest binding - showing environmental prevalence does not predict receptor-level potency. These findings support TSCA cumulative risk assessment and warrant *in vitro* phosphorylation and SMAD-reporter gene validation, subject to further studies.

Keywords: TSCA High-Priority Phthalates, Fibrosis, Computational Toxicology, Endocrine-Disrupting Chemicals, Microplastic Leachates, Molecular Docking.

1. INTRODUCTION

Uses of Plastic have increased worldwide, and it has became one of irreplaceable tool of modern life [1]. In 2022, Plastic production was estimated at 400.3 million metric tons, and it is estimated that plastic waste will rise by 13.2 billion tons in 2050 [2, 3]. Moreover, the more concerning part is only 9% of what is produced get recycled and rest add accumulates in nature. This plastic waste accumulation fragments into microplastics (MPs) less than 5 mm and in nanoplastics (NPs, collectively MNPs) [4]. These MNPs are either primary which are intentionally manufactured by the company like cosmetics and industrial applications and could be secondary which is formed by fragmentation of large plastic debris through process of mechanical, photochemical and biological degradation or weathering [4].

Of greater concern is that MNPs do not remain external to the body. Humans take them in every day through food, water, inhaled air, and skin [5]. It is estimated humans ingest tens of thousands to millions of particles per year - which is equivalent to several milligrams per day [6]. Through inhalation and skin contact alone, phthalate intake from MNPs ranges from 1.2 to 13 ng/kg body weight per day indoors [7]. Smaller particles penetrate deeper into biological

*Address correspondence to this author at the Department of Zoology, School of Basic & Applied Science, Sanskaram University, Patauda-124108, Jhajjar, Haryana, India; Tel: +91-8814810700; E-mail: Naveentak72@gmail.com

†Equal Authors

ISSN: 1929-2260 / E-ISSN: 1929-2279/26

tissues. MPs less than 20 μm penetrate biological membranes and organs, and MPs less than 10 μm cross cell membranes and even the placental barrier [6]. MNPs have now been confirmed in human brain, liver, kidney, blood, lungs, placenta, and fetal organs [4, 8, 9]. Brain tissue showed higher concentrations than liver or kidney, and concentrations in all three organs increased significantly from 2016 to 2024 - showing that the body burden is rising [8]. Moreover, MNPs were found in arterial plaques of 58.4% of patients undergoing carotid endarterectomy - these patients showed a hazard ratio of 4.53 for myocardial infarction, stroke, or death at 34 months - the first direct evidence in humans linking MNP accumulation in tissue to cardiovascular events [10].

These MNPs do not act alone. They carry plastic additives which leach continuously from the polymer surface into surrounding biological environments. Among these additives, phthalate esters are the most abundantly detected class in human biomonitoring globally [11]. Phthalates are not covalently bonded to the plastic polymer which leads to their continuous release under normal body conditions of temperature, pH, and water contact [11, 12]. They are lipophilic in nature which leads to partitioning into fat tissue and biological membranes, along with crossing of the placental barrier [12]. DEHP alone accounts for approximately 40% of global plasticizer consumption, and DBP, DIBP, and DEHP are among the most detected phthalates in water, sediment, and food worldwide [11]. In human biomonitoring, DEHP metabolites are detected at nanomolar to low micromolar concentrations in plasma and urine, DBP metabolites in approximately 98% of individuals sampled, and BBP metabolites in 97–99% of women and children [13, 14].

These chemicals are thus detectable in virtually all human individuals, yet their molecular-level biological effects remain incompletely characterized. Seven phthalates - DEHP, DBP, DIBP, BBP, DCP, diisononyl phthalate (DINP), and diisodecyl phthalate (DIDP) - are currently under active federal risk evaluation by the US EPA under TSCA, designated as High-Priority Substances based on established health concern [15]. Among these seven, five - DEHP, DBP, DIBP, BBP, and DCP - were selected here based on dominance in environmental detection and human biomonitoring data [13, 14, 16]. Humans are exposed to all five together not one at a time, and evidence supports that phthalate mixture exposures act additively on common biological targets - which leads to single-compound risk assessments likely underestimating real-world risk [16]. DEHP is classified Group 2B - possibly carcinogenic - by IARC, with tumor-promoting activity in breast, thyroid, ovarian, and prostate cancers through Notch, Wnt, TGF-β, and NF-κB signaling pathways [17]. BBP, DBP, and DEHP at 10–100 nM increased cell viability, reduced apoptosis, and promoted cancer stem cell markers in breast cancer cells via PI3K/AKT/mTOR upregulation [18]. DEHP linked to pancreatic ductal adenocarcinoma through a KLF5-centered adverse outcome pathway involving PI3K-AKT and MAPK signaling [19]. Phthalates also interfere with estrogen and androgen receptors - DEHP and DBP showed highest predicted endocrine disruption risk - which leads to DNA damage in spermatozoa, epigenetic changes, and reproductive disorders in both sexes [5, 20]. At cardiovascular level, DEHP linked to oxidative stress, metabolic dysfunction, and cardiovascular mortality globally [21].

Researchers have started using computational approaches to understand how these phthalates interact with disease-relevant proteins. Molecular docking and network toxicology studies have linked DEHP to cancer targets across breast, prostate, renal, lung, colorectal, gastric, and thyroid cancers [22-30], each study shows compound-specific interactions. We previously proposed for the first time that MNPs can cause lymphoma in our recent paper [31]. But each study tested one compound against one target. None tested all these five phthalates together and covered a complete signaling pathway from membrane receptor to cytoplasmic transducer to nuclear effector at the same time. The molecular basis of how these five compounds collectively engage to any pathway remains unknown.

Therefore, we docked all five - DEHP, DBP, DIBP, BBP, and DCP - against four canonically resolved protein targets of TGF-β/SMAD signaling Pathway - TGFβRI, TGFβRII, SMAD2, and SMAD3/SMAD4 - the only pathway among highest-studied candidates with crystallographically resolved targets across all three cellular compartments - providing a systematic comparative framework for future *in vitro* and *in vivo* validation using AutoDock 4 and AutoDock Vina. AutoDock 4 employs a Lamarckian Genetic Algorithm with empirical free energy scoring, while AutoDock Vina uses gradient-based optimization with an improved scoring function; concurrent use of both engines improves confidence in predicted binding poses by assessing concordance across two independent scoring functions, as both have demonstrated concordance with experimentally determined affinities across diverse ligand-receptor systems [32, 33].

2. MATERIALS AND METHODOLOGY

2.1. Ligand and Pathway Selection Rationale

Five phthalate esters-DEHP, DBP, DIBP, BBP, and DCP-were selected as all five are currently designated as High-Priority Substances under active risk evaluation by the US EPA under TSCA (2019) [15]. To find the most suitable signaling pathway for docking these five phthalates, PubMed was searched using "phthalates" combined with 18 major human signaling pathways. The number of results were given in brackets - NF-κB (341), p53 (188), TGF-β (154), Estrogen Receptor (130), Androgen Receptor (99), AhR (60), Notch (37), Wnt/β-catenin (36), AMPK (32), PI3K/AKT/mTOR (26), JAK/STAT (21), Nrf2/Keap1 (4), cGAS-STING (4), Hippo/YAP (1), PPARγ/PPARα (1), and Hedgehog/Gli, EGFR/RTK, and MAPK/ERK/ JNK/p38 (0 each). Top five-NF-κB, p53, TGF-β, Estrogen Receptor, and Androgen Receptor-were shortlisted for further evaluation. Now, as phthalates are lipophilic in nature, they can penetrate and bind across all three cellular compartments-membrane surface receptors, cytoplasmic mediators, and nuclear components. Each shortlisted pathway was therefore checked for protein targets across all three compartments. NF-κB has no defined membrane receptor. p53 has no membrane component. Estrogen Receptor and Androgen Receptor are intracellular nuclear receptors with no membrane receptor in their canonical axis. Only the canonical TGF-β/SMAD signaling Pathway have all three components-TGFβRI and TGFβRII at the membrane, SMAD2 in the cytoplasm, and SMAD3/SMAD4 at nuclear interface-and was therefore selected as docking target for this study. 2D structures were drawn in ACD/ChemSketch and 3D conformers were retrieved from PubChem and later visualized in UCSF Chimera (Figure **1**).

2.2. Protein Structure Retrieval and Preprocessing

Four high-resolution X-ray crystal structures covering canonical TGF-β signaling Pathway were selected for docking-TGF-βR1 (PDB: 3TZM), TGF-βR2 (PDB: 5E92), SMAD2 (PDB: 1DEV), and SMAD3/SMAD4 heterodimer (PDB: 1U7F) (Table **1**). All structures were downloaded in *.pdb* format from the RCSB Protein Data Bank and processed in AutoDock Tools (ADT) v4.0 [32]. Preprocessing involved-removal of crystallographic water molecules, co-crystallized ligands, metal ions, and non-standard residues, addition of polar hydrogens to reflect physiological protonation, and third assignment of Kollman united-atom charges for AutoDock force-field compatibility. Each receptor was then converted to *.pdbqt* format for downstream docking. Binding site coordinates were determined using literature-validated active site residues and visually confirmed in ADT (Table **1**).

2.3. Ligand Structure Preparation

All five ligands were prepared by first drawing their 2D molecular frameworks in ACD/ChemSketch. 3D conformers were then retrieved from PubChem (https://pubchem.ncbi.nlm.nih.gov/) for geometry confirmation and energy minimization. Moreover, preprocessing in AutoDock Tools v4.0 involved assigning Gasteiger partial charges to all atoms and defining rotatable bonds to introduce torsional flexibility. Final ligand structures were saved in .pdbqt format for compatibility with both docking engines.

2.4. Molecular Docking Protocol

A dual-docking workflow-AutoDock Vina (v1.1.2) and AutoDock 4 (v4.2.6)-was used to get concordant binding affinity data across two independent computational docking approaches for all five phthalates against the four TGF-β pathway targets. AutoDock 4 uses a Lamarckian Genetic Algorithm (LGA) for conformational sampling, while AutoDock Vina uses an efficient scoring function for pose prediction- running both together allows assessment of concordance between two independent computational algorithms [32, 33]. A uniform grid box of 40 × 40 × 40 $Å^3$ was applied to all four targets with grid-point spacing of 0.5 Å, centered on literature-validated active site residues (Table **1**). Docking in Vina used exhaustiveness = 8. AutoDock 4 used 60 independent LGA runs per ligand-receptor pair with population size of 350 and maximum evaluations of 3×10^5. Ligands were provisionally classified as predicted binders when estimated binding free energy (ΔG) was ≤ −6.0 kcal mol^{-1} - a widely used computational threshold that is method-dependent and does not constitute experimental confirmation of binding [34, 35]. Lowest-energy pose for each ligand-target pair was kept for interaction analysis.

2.5. Binding Site Definition and Interaction Profiling

Binding pockets for all four targets were delineated using a hybrid experimental-computational approach. For TGF-βR1, the co-crystallized inhibitor SB431542 guided grid-center coordinates and residue boundaries. For TGF-βR2, SMAD2, and SMAD3/SMAD4, binding cavities were predicted in Discovery Studio Visualizer (DSV) and cross-checked with published structural reports (Table **1**). Grids encompassed canonical ATP-binding clefts, receptor interface grooves, and SMAD

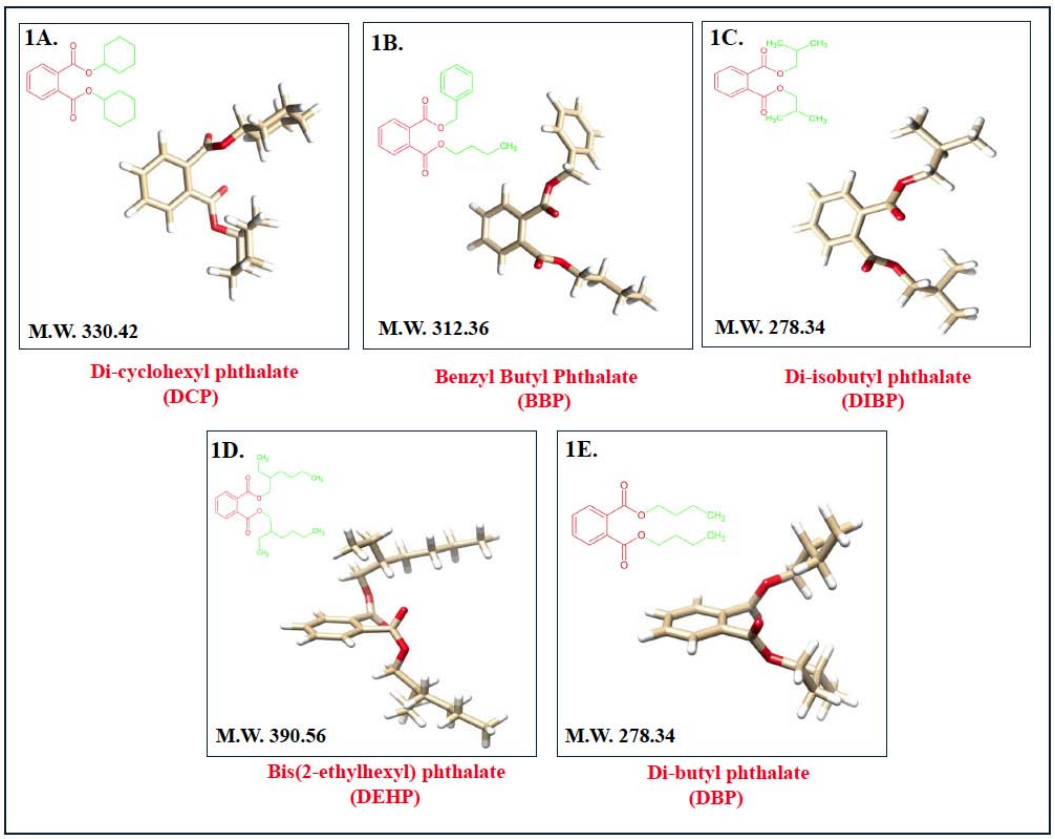

Figure 1: 2D and 3D structure of five selected phthalates. (**1A**) Di-cyclohexyl phthalate (DCP); (**1B**) Benzyl butyl phthalate (BBP); (**1C**) Di-isobutyl phthalate (DIBP); (**1D**) Bis(2-ethylhexyl) phthalate (DEHP); and (**1E**) Di-butyl phthalate (DBP). All five are currently under active federal risk evaluation as High-Priority Substances under TSCA (1). 2D structure shown in top left was drawn using ACD/ChemSketch where core phthalate is in red and side chain in green. 3D structure was retrieved from PubChem and later visualized in UCSF Chimera.

Table 1: Active Site Amino acids of TGF-βR1, TGF-βR2, SMAD2, and SMAD3/4 used for Molecular Docking

Receptor Name	PDB-ID	Docking Grid Parameters	Active sites amino acids	Reference
TGF-βR1	3TZM	Grid box size: 40 × 40 × 40 Å³ Grid center: (6.149, 7.966, 6.279) Grid spacing: 0.500 Å	ILE211A, GLY214A, ARG215A, ALA230A, LYS232A, LEU260A, LEU278A, SER280A, ASP281A, TYR282A, HIS283A, LYS335A, LYS337A, ASN338A, LEU340A, ASP351A	[59]
TGF-βR2	5E92	Grid box size: 40 × 40 × 40 Å³ Grid center: (16.922, -1.091, 8.339) Grid spacing: 0.400 Å	GLY251A, GLY253A, ARG254A, PHE255A, ALA256A, VAL258A, ALA275A, LYS277A, LEU305A, THR325A, ALA326A, PHE327A, HIS328A, ASN332A, ASP379A, LYS381A, SER383A, ASN384A, LEU386A, ASP397A	[60]
SMAD 2	1DEV	Grid box size: 40 × 40 × 40 Å³ Grid center: (48.474, 103.158, 45.743) Grid spacing: 0.400 Å	TYR341, ILE343, PHE348, TYR366, TRP368, CYS374, LYS375, ASN381	[61]
SMAD3/4	1U7F	Grid box size: 40 × 40 × 40 Å³ Grid center: (-25.742, 64.334, 55.089) Grid spacing: 0.400 Å	SMAD3: LYS341, LYS345, LYS439, ARG438 SMAD4: LYS419, TYR425, ARG427, ARG377	[62]

MH2 domains known to mediate small-molecule modulation within TGF-β Pathway. Each grid fully enclosed functionally relevant residues to capture both catalytic and allosteric interactions.

Moreover, top-ranked docking complexes were imported into DSV for interaction analysis. 2D contact maps and 3D overlays were generated to visualize all molecular contacts. Interactions were categorized by distance and geometry-hydrogen bonds (≤ 3.5 Å); vander Waals forces (≤ 4.0 Å); π -π and π -alkyl stacking; along with alkyl and C-H contacts. Color conventions followed DSV standard-hydrogen bonds in green, hydrophobic in light pink, π -interactions in purple. Color keys are given in each Figure legend.

2.6. Data Curation and Filtering

Only ligand-protein complexes showing ΔG ≤ −6.0 kcal mol^{-1} in either docking engine were retained for final comparative analysis. All metrics-binding energy, interaction type, and contacting residues-were compiled into a unified dataset. Ligands that produced no convergent binding pose under identical docking conditions are recorded as NB (No Stable/Convergent Pose) in the respective tables. Binding energy profiles were visualized using Graph pad prism (Version 9.0) as shown in Figure **2**.

3. RESULTS

3.1. Binding of Phthalates at TGF-βR1

Docking of five selected phthalates against TGF-βR1 kinase domain showed binding above the minimum threshold of −6.0 kcal/mol in both engines (Figure **2A**, **2B**). DCP showed strongest binding, −9.58 kcal/mol (AutoDock 4) and −8.5 kcal/mol (Vina). BBP followed at −7.83 and −8.0 kcal/mol. DIBP, DEHP, and

2A. TGF-Beta R1

Ligands	Binding Affinity kcal/mol (AutoDock4)	Binding Affinity (kcal/mol) (AutoDock Vina)
DCP	-9.58	-8.5
BBP	-7.83	-8.0
DIBP	-7.15	-7.6
DEHP	-6.90	-7.6
DBP	-6.96	-6.8

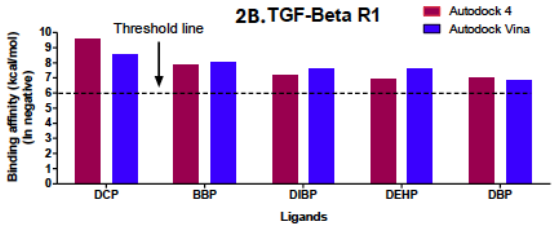

2C. TGF-BetaR2

Ligands	Binding Affinity kcal/mol (AutoDock4)	Binding Affinity (kcal/mol) (AutoDock Vina)
DCP	-9.02	-8.7
BBP	-8.34	-8.3
DIBP	-7.49	-7.0
DEHP	-6.79	-6.6
DBP	-7.23	-6.9

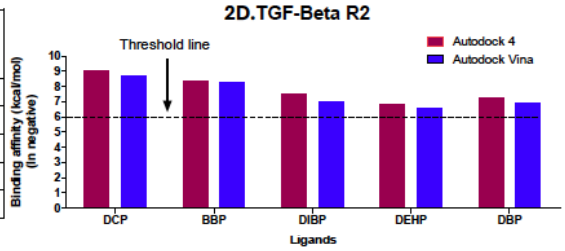

2E. SMAD2

Ligands	Binding Affinity kcal/mol (AutoDock4)	Binding Affinity (kcal/mol) (AutoDock Vina)
DCP	-6.77	-7.0
BBP	-5.54	-5.7
DIBP	-4.97	-5.5
DEHP	-4.81	-5.0
DBP	-4.41	-5.2

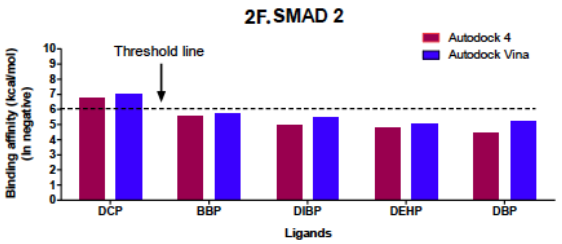

2G. SMAD3-4

Ligands	Binding Affinity kcal/mol (AutoDock4)	Binding Affinity (kcal/mol) (AutoDock Vina)
DCP	-8.15	-8.3
BBP	-7.52	-6.9
DIBP	-6.34	-6.5
DEHP	-6.15	-5.6
DBP	-6.77	-6.3

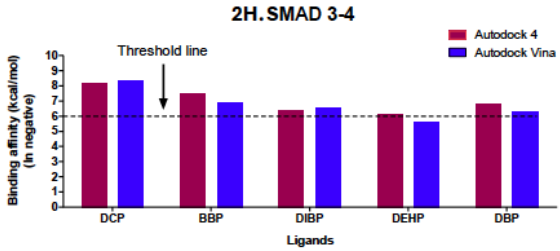

Figure 2: Binding affinity of five selected phthalates against TGF-β signaling Pathway. Binding affinity, calculated in the ΔG, kcal/mol, for the five phthalates DCP, BBP, DIBP, DEHP, and DBP were evaluated against the four target of the TGF-β signaling Pathway TGF-βR1 (**2A, 2B**), TGF-βR2 (**2C, 2D**), SMAD2 (**2E, 2F**), and SMAD3/SMAD4 (**2G, 2H**). The Binding affinity (in -ve), were calculated AutoDock 4 shown in maroon and cross verified by AutoDock Vina shown in blue, which is shown here in graph on left side and bar charts on right side. The minimum binding threshold was selected at -6.0 kcal/mol which is indicated here by a black line in right graphs. Graph pad prism was used for preparation of the graphs.

Table 2: Amino Acid-Level Mapping of Ligand-TGF-βR1 Interactions

Ligands	Interactions	Interacting-Amino Acids	Total Interacting-Amino Acids
DCP	Van der Waals Forces	ASN338A, TYR282A, HIS283A, GLY286A, ASP281A, ILE211A, VAL279A, PHE262A, GLU245A, TYR249A, LEU352A, GLY214A	21 (13 Active Site Amino Acids)
	Conventional hydrogen bond	LYS232A (1.92Å), ASP351A (1.87Å), SER280A (2.63Å)	
	Alkyl/Pi-alkyl	ALA230A, LEU340A, ALA350A, VAL219A, LEU260A, LEU278A	
BBP	Van der Waals Forces	GLY286A, HIS283A, TYR282A, ASP281A, VAL231A, VAL219A, LYS337A, ASN338A, ASP351A, GLU245A, TYR249A, PHE262A, ILE211A	20 (14 Active Site Amino Acids)
	Conventional hydrogen bond	SER280A (2.57Å), LYS232A (1.87Å)	
	Pi-Cation	LYS232A (4.15Å)	
	Pi-Sigma	LEU340A, LEU260A	
	Alkyl/Pi-alkyl	ALA350A, ALA230A, LEU278A	
DIBP	Van der Waals Forces	VAL279A, VAL231A, GLU245A, TYR249A, ALA350A, LYS337A, ASN338A, GLY214A, ARG215A, VAL219A, LEU260A, ASP281A, HIS283A, TYR282A	20 (14 Active Site Amino Acids)
	Conventional hydrogen bond	SER280A (2.78Å), ASP351A (2.03Å), LYS232A (1.92Å)	
	Alkyl/Pi-alkyl	LEU278A, ALA230A, LEU340A	
DEHP	Van der Waals Forces	LYS213A, GLY214A, ASP351A, ALA350A, VAL231A, LEU260A, SER280A, GLU245A, ASP281A, TYR282A, GLY286A, GLU284A	20 (12 Active Site Amino Acids)
	Conventional hydrogen bond	LYS232A (2.58Å)	
	Pi-Sigma	VAL219A, TYR249A	
	Alkyl/Pi-alkyl	ILE211A, LEU340A, HIS283A, PHE262A, LEU278A, ALA230A	
DBP	Van der Waals Forces	VAL279A, PHE262A, GLU245A, TYR249A, SER287A, LYS337A, ASN338A, GLY286A, HIS283A, TYR282A, ASP281A, VAL219A	20 (12 Active Site Amino Acids)
	Conventional hydrogen bond	ASP351A (1.77Å), SER280A (2.01Å)	
	Pi-Sigma	LEU260A	
	Alkyl/Pi-alkyl	LEU278A, LYS232A, ALA230A, LEU340A, ALA350A	

Conventional hydrogen bond and Pi-Cation bond length are given in brackets.

DBP showed values between −6.90 to −7.15 kcal/mol across both engines.

At residue level, DCP formed highest contacts at TGF-βR1-21 total amino acids, of which 13 were active site residues (Table **2**, Figure **3A**). Three conventional hydrogen bonds formed at LYS232A, ASP351A, and SER280A, along with alkyl/π-alkyl contacts at ALA230A, LEU340A, ALA350A, VAL219A, LEU260A, and LEU278A. BBP showed 20 interacting amino acids with 14 active site contacts (Figure **3B**). Hydrogen bonds formed at SER280A and LYS232A, along with π-cation at LYS232A and π -sigma at LEU340A and LEU260A. DIBP showed 20 amino acids with 14 active site contacts and three hydrogen bonds at SER280A, ASP351A, and LYS232A (Figure **3C**). DEHP showed 20 contacts with 12 active site residues and only one hydrogen bond at LYS232A (Figure **3D**). DBP showed 20 contacts with 12 active site residues and two hydrogen bonds at ASP351A and SER280A (Figure **3E**). Moreover, SER280A, ASP351A, and LYS232A were the three recurrent active site anchors found across all five phthalates at TGF-βR1.

3.2. Binding of Phthalates at TGF-βR2

At TGF-βR2 kinase domain, all five again showed binding above −6.0 kcal/mol in both engines (Figure **2C**, **2D**). DCP again showed strongest binding-−9.02 kcal/mol (AutoDock 4) and −8.7 kcal/mol (Vina). BBP followed at −8.34 and −8.3 kcal/mol. DIBP, DBP, and DEHP showed binding between −6.79 to −7.49 kcal/mol.

At residue level, DCP formed 16 interacting amino acids at TGF-βR2 with two hydrogen bonds at ASP397A and LYS277A, along with π -sigma at VAL258A and alkyl/π-alkyl contacts at LEU305A, CYS396A, ALA275A, LEU386A, and LEU323A (Figure **4A**, Table **3**). BBP showed 17 contacts with two

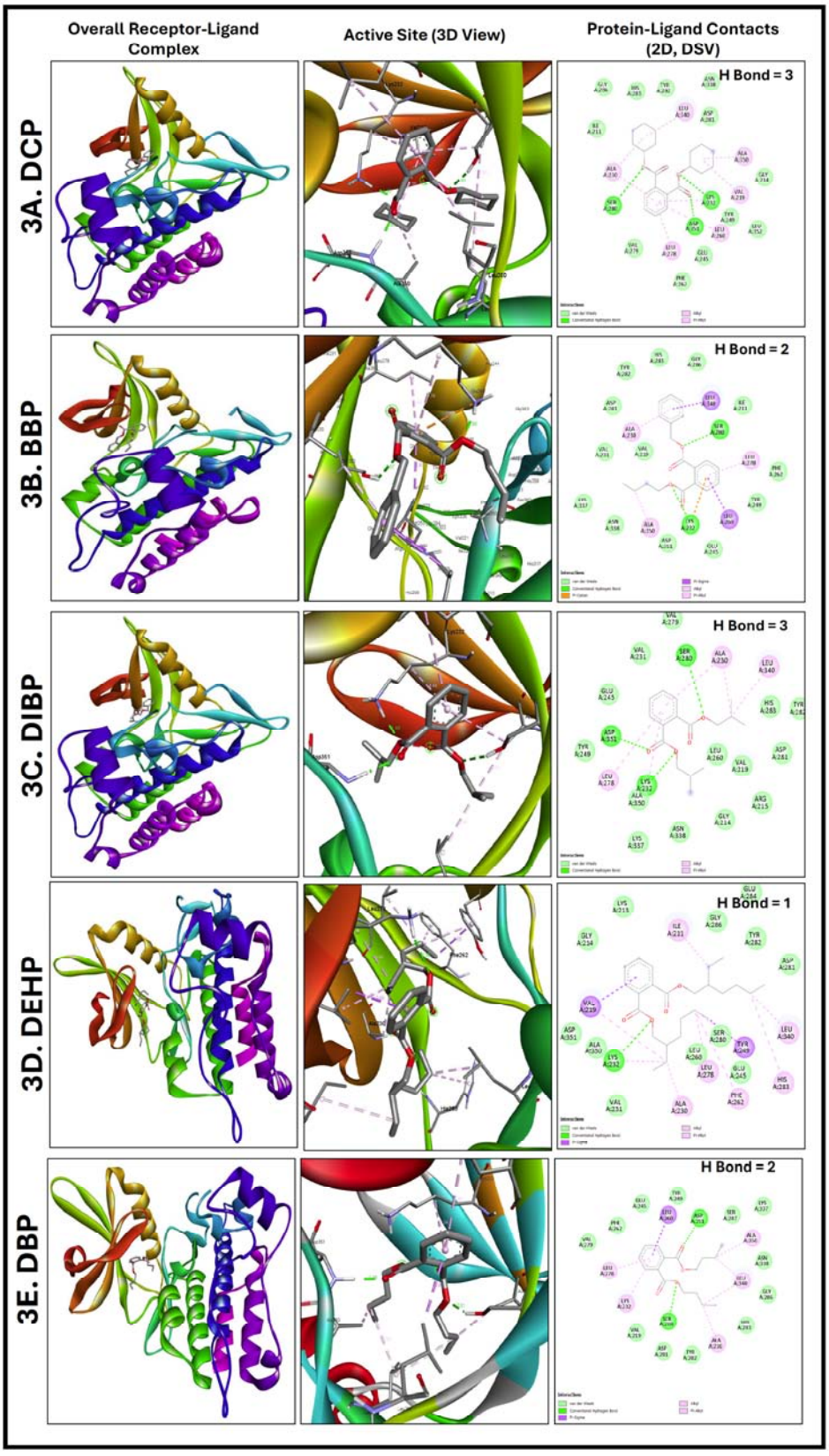

Figure 3: Binding mode of five selected phthalates at TGF-βR1 kinase domain. Five phthalates DCP (**3A**), BBP (**3B**), DIBP (**3C**), DEHP (**3D**), and DBP (**3E**) docked against the human TGF-βR1 kinase domain. For each ligand, overall receptor-ligand complex is shown on left, active site 3D view in center, and 2D protein-ligand contact map generated in Discovery Studio Visualizer (DSV) on right, annotated with total conventional hydrogen bonds (H Bond = n). Different colours indicate different interactions: Light green for vander Waals; bright green for conventional hydrogen bond; light pink for alkyl/π-alkyl; purple for π-sigma; orange for π-cation. Moreover, each residue specific interactions and bond type are given in Table **2**.

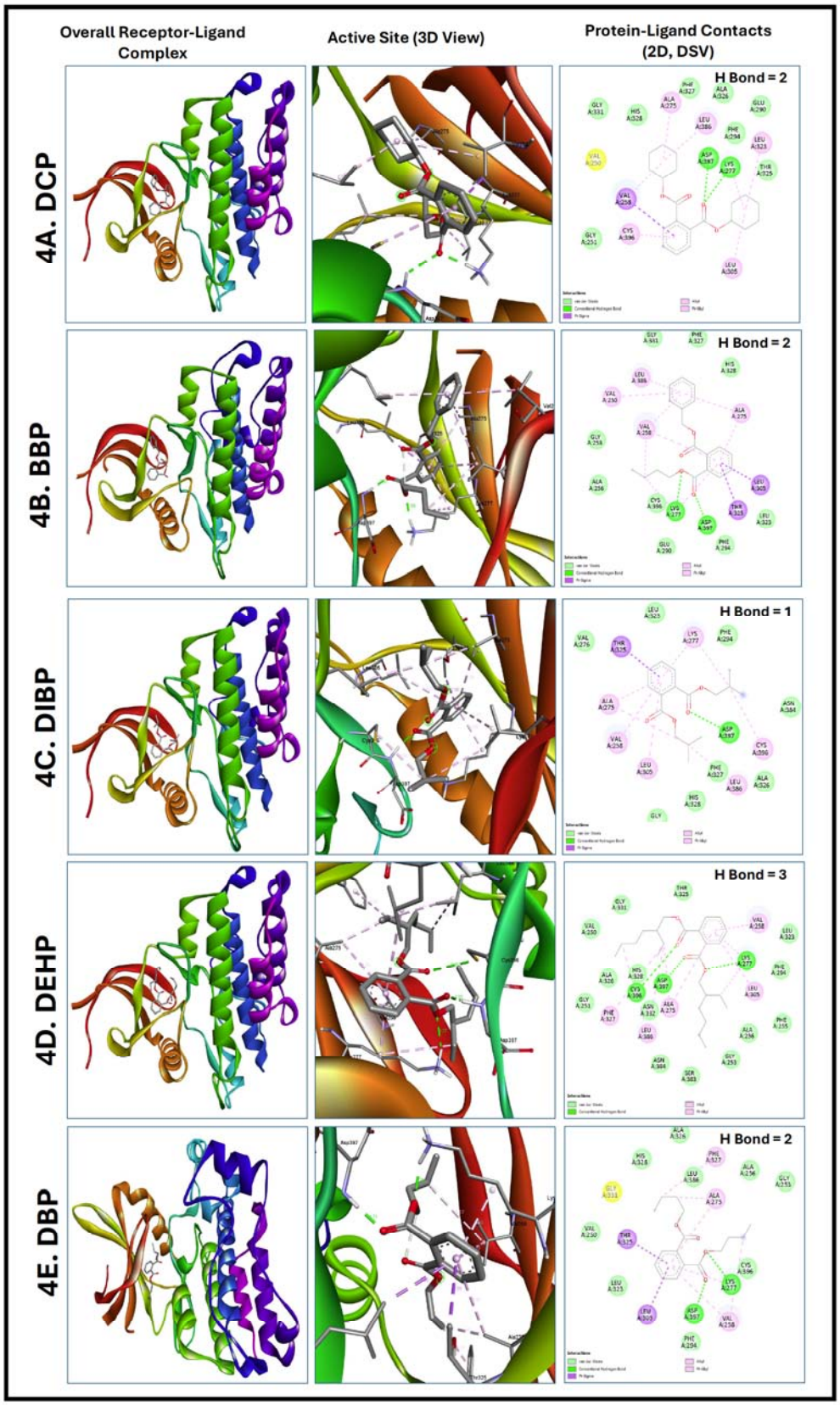

Figure 4: Binding mode of five selected phthalates at TGF-βR2 kinase domain. Five phthalates DCP (**4A**), BBP (**4B**), DIBP (**4C**), DEHP (**4D**), and DBP (**4E**) docked against the human TGF-βR2 kinase domain (PDB: 5E92). For each ligand, overall receptor-ligand complex is shown on left, active site 3D view in center, and 2D protein-ligand contact map generated in Discovery Studio Visualizer (DSV) on right, annotated with total conventional hydrogen bonds (H Bond = n). Different colours indicate different interactions: Light green for vander Waals; bright green for conventional hydrogen bond; light pink for alkyl/π-alkyl; purple for π-sigma. Moreover, each residue specific interactions and bond type are given in Table **3**.

Table 3: Amino Acid-Level Mapping of Ligand-TGF-βR2 Interactions

Ligands	Interactions	Interacting-Amino Acids	Total Interacting-Amino Acids
DEHP	Van der Waals Forces	THR325A, GLY331A, VAL250A, ALA326A, HIS328A, ASN332A, GLY251A, ASN384A, SER383A, GLY253A, ALA256A, PHE255A, PHE294A, LEU323A	21 (8 Active Site Amino Acids)
	Conventional hydrogen bond	CYS396A (3.69Å), ASP397A ((2.02Å), LYS277A (2.37Å)	
	Alkyl/Pi-alkyl	VAL258A, PHE327A, LEU386A, ALA275A	
DCP	Van der Waals Forces	GLY331A, HIS328A, PHE327A, ALA326A, GLU290A, PHE294A, THR325A, GLY251A	16 (8 Active Site Amino Acids)
	Conventional hydrogen bond	ASP397A (2.48Å), LYS277A (1.85Å)	
	Pi-Sigma	VAL258A	
	Alkyl/Pi-alkyl	LEU305A, CYS396A, ALA275A, LEU386A, LEU323A	
BBP	Van der Waals Forces	GLY331A, PHE327A, HIS328A, GLY253A, ALA256A, CYS396A, GLU290A, PHE294A, LEU323A	17 (8 Active Site Amino Acids)
	Conventional hydrogen bond	LYS277A (1.96Å), ASP397A (1.66Å)	
	Pi-Sigma	THR325A, LEU305A	
	Alkyl/Pi-alkyl	VAL258A, VAL250A, LEU386A, ALA275A	
DIBP	Van der Waals Forces	VAL276A, LEU323A, PHE294A, ASN384A, ALA326A, PHE327A, HIS328A	15 (8 Active Site Amino Acids)
	Conventional hydrogen bond	ASP397A (1.89Å)	
	Pi-Sigma	THR325A	
	Alkyl/Pi-alkyl	LYS277A, ALA275A, VAL258A, LEU305A, LEU386A, CYS396A	
DBP	Van der Waals Forces	ALA326A, HIS328A, LEU386A, VAL250A, LEU323A, PHE294A, CYS396A, GLY253A, ALA256A	16 (8 Active Site Amino Acids)
	Conventional hydrogen bond	ASP397A (1.71Å), LYS277A (1.96Å)	
	Pi-Sigma	THR325A, LEU305A	
	Alkyl/Pi-alkyl	VAL258A, PHE327A, ALA275A	

Conventional hydrogen bond length are given in brackets.

hydrogen bonds at LYS277A and ASP397A, along with π-sigma at THR325A and LEU305A (Figure **4B**). DIBP showed 15 contacts with one hydrogen bond at ASP397A (Figure **4C**). DEHP showed 21 contacts with three hydrogen bonds at CYS396A, ASP397A, and LYS277A (Figure **4D**). DBP showed 16 contacts with two hydrogen bonds at ASP397A and LYS277A (Figure **4E**). Moreover, ASP397A and LYS277A were the consistent anchor residues across all five phthalates at TGF-βR2-same pattern as seen at TGF-βR1.

3.3. Selective Predicted Binding of DCP at SMAD2 MH2 Domain

At SMAD2 MH2 domain, binding pattern differed substantially. Only DCP showed predicted binding above the −6.0 kcal/mol computational threshold -−6.77 kcal/mol (AutoDock 4) and −7.00 kcal/mol (Vina). BBP, DIBP, DEHP, and DBP produced no stable/convergent docking pose under identical conditions and are recorded as NB in Table **4**. No stable/convergent docking pose was generated for these four phthalates under the specified docking conditions.

DCP at SMAD2 formed 12 total contacts (Figure **5**, Table **4**). Vander Waals contacts found at ASN363, TRP368, PRO360, SER397, and GLN407. Two hydrogen bonds formed at MET411 and GLN364. Carbon hydrogen bond formed at LEU408, along with alkyl/π-alkyl contacts at PRO370, ARG410, ALA404, and LEU393. Moreover, TRP368-one of the key active site residues-was directly engaged by DCP via vander Waals contact. None of the remaining four phthalates contacted this residue.

3.4. Binding of Phthalates at SMAD3/SMAD4 Interface

At SMAD3/SMAD4 heterodimer, DCP again showed strongest binding-−8.15 kcal/mol (AutoDock 4) and

Table 4: Amino Acid-Level Mapping of Ligand-SMAD2 Interactions

Ligands	Interactions	Interacting-Amino Acids	Total Interacting-Amino Acids
DCP	Van der Waals Forces	ASN363, TRP368, PRO360, SER397, GLN407	12 (1 Active Site Amino Acids)
	Conventional hydrogen bond	MET411, GLN364	
	Carbon hydrogen bond	LEU408	
	Alkyl/Pi-alkyl	PRO370, ARG410, ALA404, LEU393	
BBP	NB	NB	NB
DIBP	NB	NB	NB
DEHP	NB	NB	NB
DBP	NB	NB	NB

Note: NB = No stable/convergent docking pose generated under the specified conditions. Conventional hydrogen bond length are given in brackets.

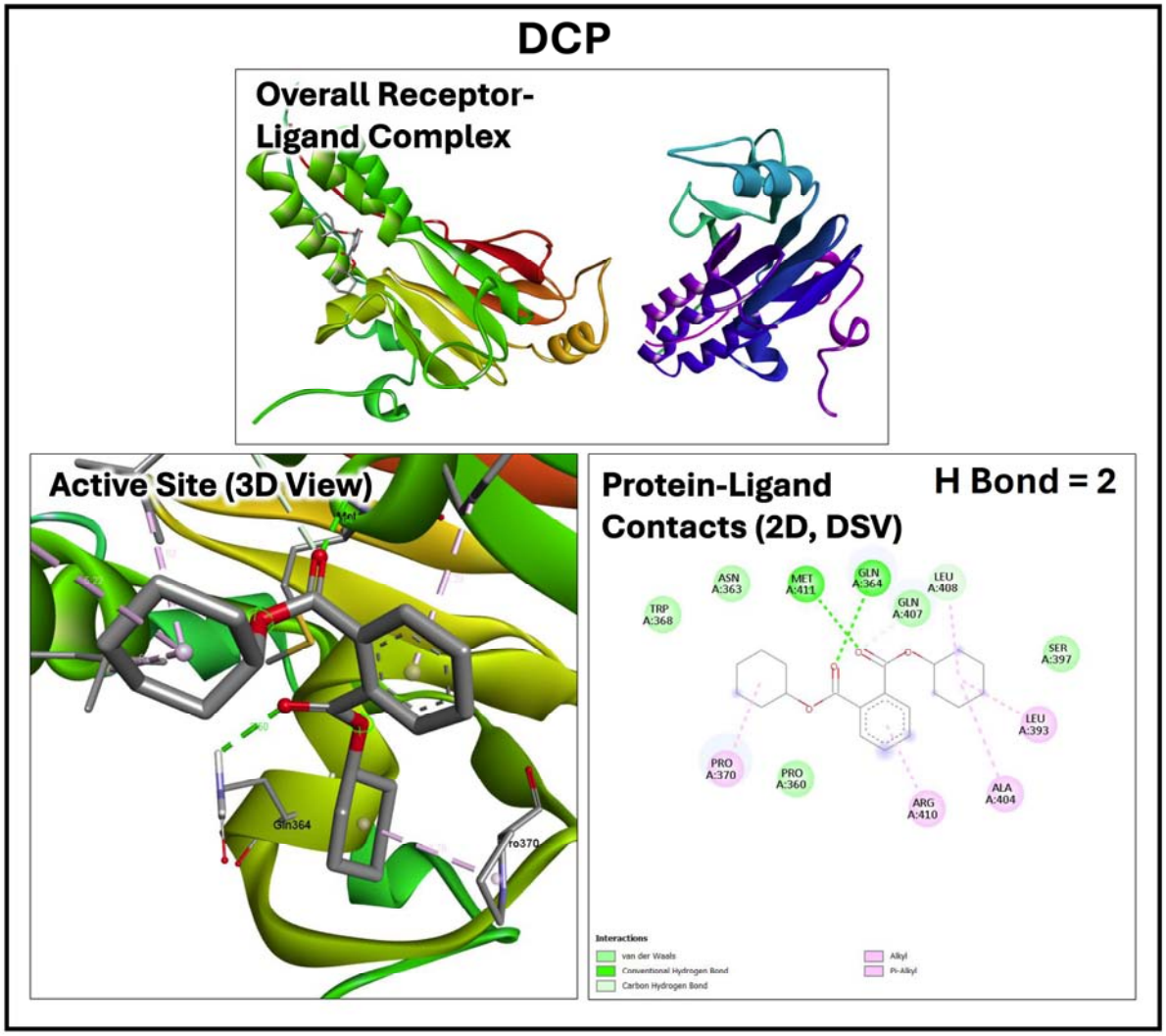

Figure 5: DCP binding at SMAD2 MH2 domain. Among the five phthalates, only DCP showed binding at SMAD2 MH2 domain (ΔG = -6.77 kcal mol⁻¹, AutoDock4; -7.00 kcal mol⁻¹, AutoDock Vina); BBP, DIBP, DEHP, and DBP showed no stable binding pose and are recorded as NB (No Binding) in Table **4**. Overall receptor-ligand complex is shown on top, active site 3D view on bottom-left, and 2D contact map generated in Discovery Studio Visualizer (DSV) on bottom-right (H Bond = 2). Different colours indicate different interactions: Light green for vander Waals; bright green for conventional hydrogen bond; light green outline for carbon hydrogen bond; light pink for alkyl; pink for π-alkyl. Moreover, each residue specific interactions and bond type are given in Table **4**.

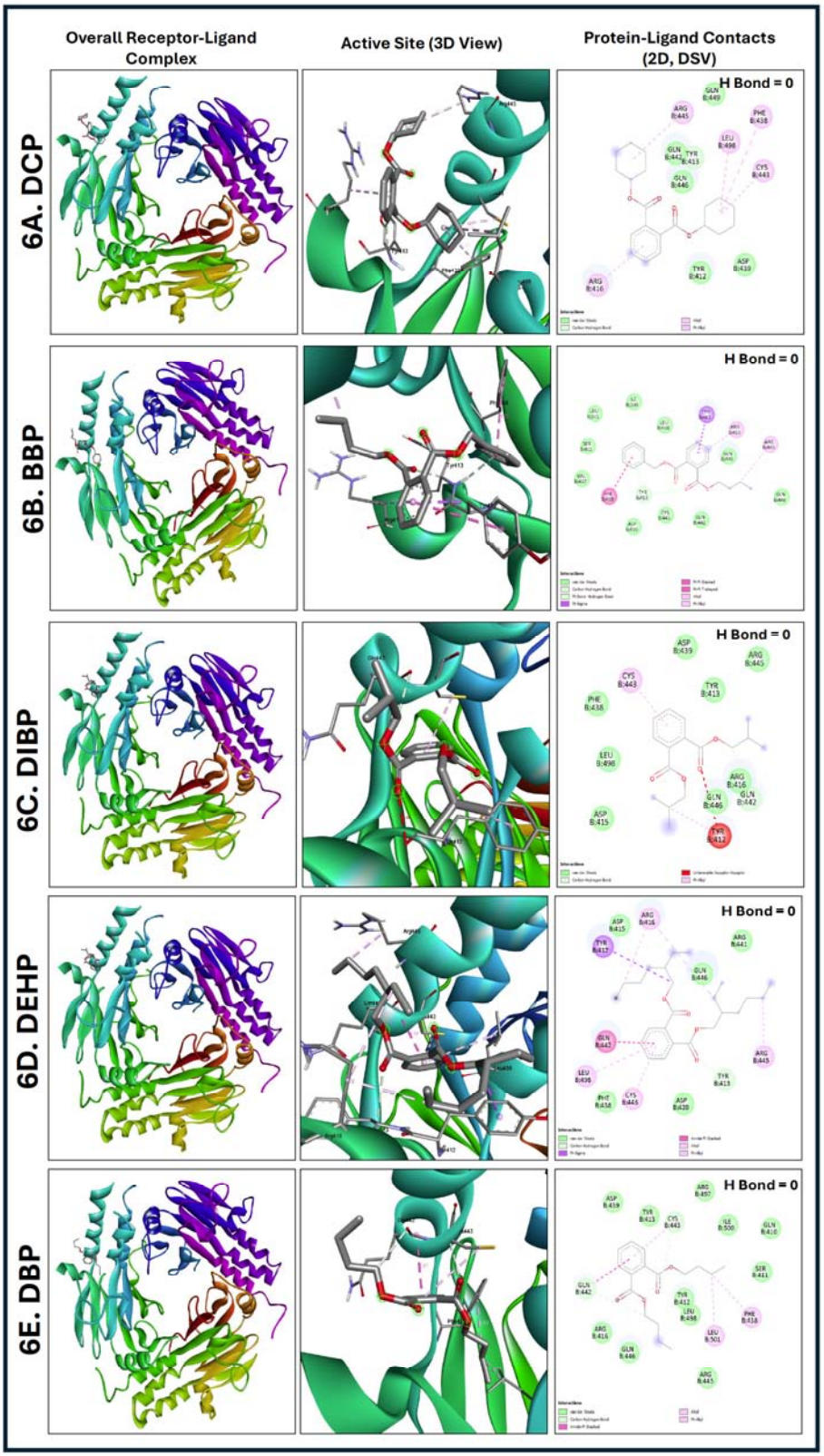

Figure 6: Binding mode of five selected phthalates at SMAD3/SMAD4 heterodimeric interface. Five phthalates DCP (**6A**), BBP (**6B**), DIBP (**6C**), DEHP (**6D**), and DBP (**6E**) docked against the SMAD3/SMAD4 heterodimer (PDB: 1U7F). For each ligand, overall receptor-ligand complex is shown on left, active site 3D view in center, and 2D contact map generated in Discovery Studio Visualizer (DSV) on right, annotated with total conventional hydrogen bonds (H Bond = n). Different colours indicate different interactions: Light green for vander Waals; bright green for conventional hydrogen bond; light green outline for carbon hydrogen bond; light pink for alkyl/π-alkyl; purple for π-sigma; dark pink for π-π stacked; orange for π-π T-shaped; yellow for amide-π stacked; red for unfavourable acceptor-acceptor (DIBP only). Moreover, each residue specific interactions and bond type are given in Table **5**.

Table 5: Amino Acid-Level Mapping of Ligand-SMAD3/4 Interactions

Ligands	Interactions	Interacting-Amino Acids	Total Interacting-Amino Acids
DEHP	Van der Waals Forces	ASP415B, ARG441B, GLN446B, ASP439B, PHE438B	12 (NIL-Active Site Amino Acids)
	Carbon hydrogen bond	TYR413B	
	Pi-Sigma	TYR412B	
	Amide-Pi stacked	GLN442B, ARG416B	
	Alkyl/Pi-alkyl	LEU498B, CYS443B, ARG445B	
DCP	Van der Waals Forces	GLN449B, GLN442B, GLN446B, TYR412B, ASP439B	11 (NIL-Active Site Amino Acids)
	Carbon hydrogen bond	TYR413B	
	Alkyl/Pi-alkyl	ARG445B, PHE438B, LEU498B, CYS443B, ARG416B	
BBP	Van der Waals Forces	ILE500B, LEU498B, LEU501B, SER411B, VAL437B, ASP439B, CYS443B, GLN442B, GLN449B, GLN446B	15 (NIL-Active Site Amino Acids)
	Carbon hydrogen bond/Pi-donor hydrogen bond	TYR413B	
	Pi-sigma	TYR412B	
	Pi-Pi Stacked/Pi-Pi T-shaped	PHE438B	
	Alkyl/Pi-alkyl	ARG416B, ARG445B	
DIBP	Van der Waals Forces	ASP439B, ARG445B, TYR413B, PHE438B, LEU498B, ASP415B, ARG416B, GLN446B	11 (NIL-Active Site Amino Acids)
	Carbon hydrogen bond	GLN442B	
	Unfavourable acceptor-acceptor	TYR412B	
	Alkyl/Pi-alkyl	CYS443B	
DBP	Van der Waals Forces	ASP439B, TYR413B, ARG497B, ILE500B, GLN410B, SER411B, TYR412B, LEU498B, ARG445B, GLN446B, ARG416B	16 (NIL-Active Site Amino Acids)
	Carbon hydrogen bond	CYS443B, GLN442B	
	Amide-Pi stacked	GLN442B	
	Alkyl/Pi-alkyl	LEU501B, PHE438B	

−8.3 kcal/mol (Vina), above − 6.0 kcal/mol threshold (Figure **2G**, **2H**). BBP followed at −7.52 and −6.9 kcal/mol. DBP showed −6.77 and −6.3 kcal/mol, DIBP showed −6.34 and −6.5 kcal/mol, and DEHP showed −6.15 and −5.6 kcal/mol.

At residue level, DCP formed 11 contacts with carbon hydrogen bond at TYR413B and alkyl/π-alkyl contacts at ARG445B, PHE438B, LEU498B, CYS443B, and ARG416B (Figure **6A**, Table **5**). BBP showed 15 contacts with carbon hydrogen bond at TYR413B, π -sigma at TYR412B, π -π stacked/T-shaped at PHE438B, along with alkyl/π-alkyl contacts at ARG416B and ARG445B (Figure **6B**). DIBP showed 11 contacts with carbon hydrogen bond at GLN442B and an unfavourable acceptor-acceptor interaction at TYR412B-the only unfavourable interaction found across all five phthalates at this target (Figure **6C**). DEHP showed 12 contacts with carbon hydrogen bond at TYR413B, π-sigma at TYR412B, along with amide-π stacked contacts at GLN442B and ARG416B (Figure **6D**). DBP showed 16 contacts with carbon hydrogen bond at CYS443B and GLN442B, along with amide-π stacked at GLN442B (Figure **6E**). Moreover, none of the five phthalates engaged the canonical active site residues of SMAD3-LYS341, LYS345, LYS439, ARG438-or SMAD4-LYS419, TYR425, ARG427, ARG377. All binding poses localized to a peripheral region of heterodimeric interface rather than canonical MH2 active site. The biological significance of these peripheral interface interactions therefore remains uncertain and should not be interpreted as evidence of canonical pathway disruption without experimental validation.

4. DISCUSSION

Our criteria selected TGF-β/SMAD signaling Pathway to study against these five phthalates. TGF-β-transforming growth factor-beta-controls how cells

grow, divide, and die [35-37]. Under normal conditions it acts as a tumor suppressor, however, when chronically disrupted-by mutations, inflammation, or environmental chemicals-the same pathway switches and starts promoting cancer, fibrosis, and immune evasion [36, 37]. This contextual switch underlies its pathological significance. The canonical TGF-β/SMAD Pathway operates through a linear cascade-TGF-β binds TGFβRII at cell surface, activates TGFβRI, which phosphorylates SMAD2 and SMAD3 inside the cell, which then join SMAD4 and move into nucleus to switch fibrosis and oncogene-related genes on or off [36, 38]. All five phthalates crossed the −6.0 kcal mol^{-1} binding threshold at TGFβRI, TGFβRII, and SMAD3/SMAD4 in both AutoDock 4 and AutoDock Vina- yielding concordant binding affinity data across both computational engines. Each compound exhibited a distinct binding profile.

DEHP. DEHP showed binding at all four targets-weakest of the five but still above threshold at TGFβRI (−6.90 kcal mol^{-1}), TGFβRII (−6.79 kcal mol^{-1}), and SMAD3/SMAD4 (−6.15 kcal mol^{-1}). Only one hydrogen bond formed at TGFβRI at LYS232A along with twelve vander Waals contacts. DEHP is the most globally produced phthalate-nearly 50% of worldwide plasticizer production-and its metabolites are detected in virtually all individuals sampled at nanomolar to low micromolar concentrations [11, 39]. Despite being the most environmentally prevalent, it showed the weakest TGF-β pathway binding of the five. These results suggest that, detection frequency does not predict receptor-level potency. Experimentally, DEHP is the most studied of the five at TGF-β level. Study by Kim *et al*. showed DEHP induced proliferation, migration, stemness, and EMT in human endometrial and endometriotic epithelial cells via TGF-β/SMAD signaling-confirmed when selective TGFβR1/2 inhibitor LY2109761 reversed all DEHP-induced effects under experimental conditions [40]. Study by Liu *et al*. showed prenatal DEHP exposure upregulated TGF-β1 expression in fetal mouse genital tubercles confirmed by RT-PCR and Western blot [41]. Study by Zhou *et al*. showed gestational DEHP exposure reduced urethral EMT by suppressing TGF-β/SMAD signaling in rats-and TGF-β1 restored EMT by activating the same Pathway [42]. The experimental evidence for DEHP at TGF-β level is therefore the strongest among the five.

DBP. DBP showed binding at TGFβRI (−6.96 kcal mol^{-1}), TGFβRII (−7.23 kcal mol^{-1}), and SMAD3/SMAD4 (−6.77 kcal mol^{-1})-above threshold at all three-forming two hydrogen bonds at TGFβRI and TGFβRII each. DBP metabolites are detected in approximately 98% of all individuals sampled in large-scale biomonitoring programs [13]. Study by Hua *et al*. showed DBP increased NAP-2 secretion from vascular endothelium which promoted EMT in urothelial cells through TGF-β Pathway-and TGF-β inhibitor LY219761 blocked this DBP-induced EMT directly, confirming TGF-β dependency [43]. DBP also suppressed TGFB1I1-TGF-β1 inducible interacting protein-in hypospadias offspring, further linking it to TGF-β system components at molecular level [11]. The docking findings here are therefore directly supported by experimental evidence for DBP at TGF-β level.

DIBP. DIBP showed binding at TGFβRI (−7.15 kcal mol^{-1}), TGFβRII (−7.49 kcal mol^{-1}), and SMAD3/SMAD4 (−6.34 kcal mol^{-1})-above threshold and stronger than DBP at TGFβRII. Three hydrogen bonds formed at TGFβRI-same number as DCP-at SER280A, ASP351A, and LYS232A. DIBP is increasing rapidly in human biomonitoring as a direct replacement for DBP, with equivalently high human exposure risks [11]. However, no individual experimental study linking DIBP alone to TGF-β signaling has been published so far- representing a notable gap in the literature [44]. Study by Shukla *et al*. showed that a phthalate mixture containing DEHP, BBP, DBP, DIBP, and DEP elevated TGF-β signaling in mouse uterine tissue after 6 months of chronic dietary exposure confirmed by RNA-sequencing and validated by qPCR, along with collagen deposition and uterine stiffness confirmed by Second Harmonic Generation imaging [45]. DIBP was a named component of that mixture. This computational study is therefore the first to provide any individual molecular-level evidence that DIBP directly engages TGF-β pathway receptor proteins. Future *in vitro* studies using TGFβRI kinase phosphorylation assays and SMAD2 reporter gene systems with DIBP alone are warranted to experimentally confirm this predicted engagement.

BBP. BBP showed strong binding at TGFβRI (−7.83 kcal mol^{-1}), TGFβRII (−8.34 kcal mol^{-1}), and SMAD3/SMAD4 (−7.52 kcal mol^{-1})-second only to DCP at every target. Two hydrogen bonds formed at TGFβRI and TGFβRII each, along with π-sigma and π-cation contacts. BBP metabolites are detected in 97–99% of individuals sampled in population-wide biomonitoring programs and the US EPA classifies it as a possible human carcinogen [46]. No direct TGF-β mechanistic study exists for BBP individually. However, study by Wang *et al*. showed BBP induced lung injury and fibrosis through neutrophil extracellular trap

formation-and TGF-β/SMAD is the established central mediator of this kind of fibrogenic cascade [26, 47]. Study by Wang *et al*. also showed BBP promoted breast cancer stem cell expansion and EMT via AhR/SPHK1 signaling-confirming its oncogenic potential through EMT activation, a hallmark of TGF-β-driven cancer progression [48]. The docking evidence here provides the first molecular-level rationale for why BBP may engage TGF-β pathway directly.

DCP. DCP showed strongest binding of all five across all four targets-−9.58 kcal mol^{-1} at TGFβRI, −9.02 kcal mol^{-1} at TGFβRII, −6.77 kcal mol^{-1} at SMAD2, and −8.15 kcal mol^{-1} at SMAD3/SMAD4. The reason is its two rigid cyclohexyl rings which fit into the hydrophobic pockets of TGF-β kinase domains without the conformational flexibility penalty that limits linear chain compounds [49, 50]. DCP is the only compound that produced a predicted binding pose at the SMAD2 MH2 domain. BBP, DIBP, DBP, and DEHP all four produced no convergent binding pose under identical docking conditions. Only DCP's cyclohexyl geometry reached TRP368-a key active site residue which none of the other four phthalates reached. This is significant because SMAD2 phosphorylation by activated TGFβRI drives SMAD4 association, nuclear translocation, and

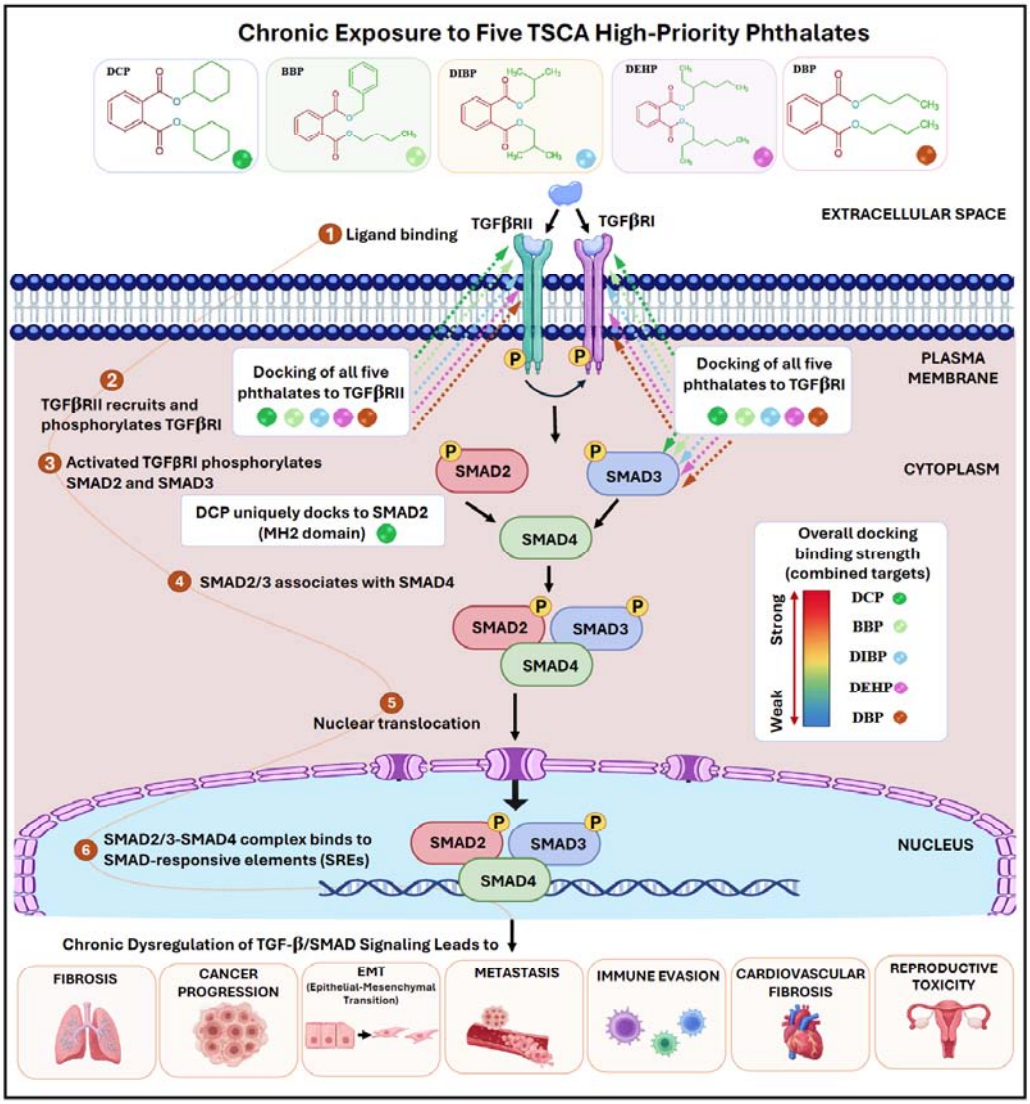

Figure 7: Graphical summary of docking of five TSCA High-Priority phthalates against canonical TGF-β/SMAD signaling Pathway. Top panel shows 2D structures of five selected phthalates - DCP, BBP, DIBP, DEHP, and DBP - color coded by overall docking binding strength across all four targets from strong to weak as DCP > BBP > DIBP > DEHP > DBP. Steps 1–6 show the canonical TGF-β/SMAD signaling cascade from extracellular ligand binding at TGFβRII and TGFβRI at plasma membrane, through cytoplasmic SMAD2/3 phosphorylation and SMAD4 association, to nuclear translocation and SMAD-responsive element binding. Colored dotted arrows show docking of all five phthalates to TGFβRI and TGFβRII, while DCP uniquely docked to SMAD2 MH2 domain in cytoplasm. Chronic dysregulation of this Pathway by phthalate binding leads to fibrosis, cancer progression, EMT, metastasis, immune evasion, cardiovascular fibrosis, and reproductive toxicity as shown in bottom panel.

transcription of fibrosis genes including collagen type I, α-SMA, MMP1, and LOXL1 [51]. A ligand at the SMAD2 MH2 interface could alter this entire process. DCP is therefore the only tested phthalate predicted to interact with TGF-β pathway components at three levels simultaneously-membrane receptor, cytoplasmic transducer, and peripheral nuclear heterodimer interface-though the functional significance of the SMAD3/SMAD4 peripheral interaction remains to be experimentally established. DCP is also the least detected of the five in routine biomonitoring-yet it showed the strongest predicted molecular engagement with TGF-β pathway proteins. This structure-activity observation - attributable to its rigid bicyclic cyclohexyl geometry - is hypothesis-generating and should not be interpreted as evidence of greater real-world risk; molecular potency in silico and actual exposure burden are distinct parameters, and DCP's lower biomonitoring prevalence means population-level risk requires separate epidemiological and toxicokinetic evaluation. No experimental TGF-β study existed for DCP before this work. However, study by Ganesh *et al*. showed DCP activates multiple human nuclear receptors in HepG2 cells through preferential interaction with hydrophobic amino acids in receptor binding pockets-confirming DCP has the molecular characteristics needed to engage structured hydrophobic receptor cavities, consistent with what is found here at TGF-β pathway targets [52]. Moreover, EPA has confirmed DCP presents unreasonable risk of injury to human health and included it in cumulative phthalate risk assessment [53]. These computational findings provide a preliminary molecular-level basis for understanding why. Given DCP's unique three-level predicted engagement - at TGFβRI, TGFβRII, and SMAD2 simultaneously - targeted *in vitro* phosphorylation assays, SMAD-reporter gene validation, and *in vivo* combinatorial exposure studies with DCP are strongly recommended as priority future investigations.

Taken together, phthalates have been directly detected in circulating human blood and lymphoid tissues-the precise anatomical compartments where TGF-β/SMAD signaling is most active [54]. These phthalates are not just theoretically capable of reaching TGF-β pathway targets. They are physically present within these compartments. If chronic phthalate exposure does bias TGF-β/SMAD signaling-as our computational docking data and supporting experimental evidence from other studies collectively suggest, and subject to experimental confirmation particularly regarding the peripheral SMAD3/SMAD4 interface engagement-the disease consequences may span the full range of TGF-β-linked pathology . At fibrotic level, TGF-β/SMAD drives fibroblast-to-myofibroblast differentiation across lung, liver, kidney, and heart (Figure **7**) [26, 37, 55]. At oncogenic level, chronic dysregulation drives EMT, invasion, metastasis, angiogenesis, and immune evasion-with loss-of-function mutations in TGFBR1, TGFBR2, SMAD2, SMAD3, and SMAD4 frequent in pancreatic, colorectal, and breast cancers [36, 56]. At cardiovascular level, TGF-β is elevated in myocardial fibrosis, valve fibrosis, and arteriosclerosis-and DEHP has already been epidemiologically associated with cardiovascular mortality [21, 57, 58]. At reproductive and developmental level, DEHP and DBP modulate TGF-β/SMAD pathway components in urethral, uterine, and gonadal tissues (Figure **7**) [41, 42, 45].

5. LIMITATIONS

Several limitations of this study warrant explicit acknowledgment. First, all four protein structures were used in rigid or mostly static form during docking, which does not account for induced-fit conformational changes under physiological conditions. Second, docking scores are inherently method-dependent and predictive - they do not equate to experimentally measured binding affinities and carry intrinsic uncertainty. Third, molecular dynamics simulations were not performed, meaning the stability of predicted binding poses over time remains unverified. Fourth, no experimental affinity measurements were conducted to validate the computational predictions. Fifth, it remains to be established whether the predicted binding poses at TGFβRI, TGFβRII, SMAD2, and the peripheral SMAD3/SMAD4 interface actually alter receptor kinase activity or SMAD phosphorylation. These limitations underscore that the findings presented here are hypothesis-generating computational observations requiring experimental confirmation.

6. CONCLUSION

Overall, we found herein that all five phthalates demonstrate predicted binding to TGF-β pathway proteins as a computationally identified common molecular interaction. These computational findings demonstrate shared predicted engagement of common TGF-β pathway targets across all five phthalates, which is consistent with - but does not itself demonstrate - the biological additivity argument that co exposure risk may exceed that of individual compounds; experimentally demonstrated mixture additivity remains to be established [16]. DCP showed the strongest predicted TGF-β pathway binding and

unique predicted SMAD2 domain engagement despite being the least detected phthalate in routine biomonitoring. A compound rarely detected in biomonitoring thus showed the strongest predicted receptor-level potency - reinforcing that environmental prevalence does not predict molecular potency. These findings are subject to in vitro phosphorylation and SMAD-reporter gene validation, molecular dynamics simulations, and in vivo combinatorial exposure studies. Moreover, based on shared engagement of common binding residues - particularly SER280A and ASP351A at TGFβRI and ASP397A and LYS277A at TGFβRII across all five phthalates - additive or potentially synergistic interference at these anchor points is hypothetically plausible under co-exposure conditions but cannot be inferred from independent single-compound docking alone; however, competitive binding at overlapping sites cannot be excluded and whether interactions are ultimately additive, synergistic, or antagonistic requires experimental confirmation through in vitro co-exposure phosphorylation assays and SMAD-reporter gene studies. These five TSCA High-Priority phthalates may warrant consideration not only as reproductive and developmental toxicants but as candidate allosteric modulators of the most consequential dual-role signaling Pathway in human biology, subject to further studies.

ETHICS APPROVAL AND CONSENT TO PARTICIPATE

Not applicable.

CONSENT FOR PUBLICATION

Not applicable.

AVAILABILITY OF DATA AND MATERIALS

All data generated or analyzed during this study are included in this published article. Raw docking output files and interaction data will be made available from the corresponding author upon reasonable request.

DECLARATION OF CONFLICTING INTEREST

The Author(s) declare(s) that there are no relevant financial or non-financial competing interests to report.

FUNDING

This research received no specific grant from any funding agency in the public, commercial, or not-for-profit sectors.

AUTHOR'S CONTRIBUTION

Mrinmoy Mandal: Conceptualization, Methodology, Software, Formal Analysis, Writing - Original Draft. **Naveen Kumar:** Conceptualization, Supervision, Writing - Review & Editing, Project Administration. **Pooja Kadyan**: Review & Editing, Validation. **Sapna Redhu** - Review & Editing, Validation. **Jayendra Kumar Singh**: Review & Editing, Validation. **Kaushalendra:** Review & Editing, Validation. **Nisha Yadav:** Data Curation, Visualization. **Divya Tyagi:** Validation, Resources. **Vikrant:** Investigation, Software. **Varsha Singh:** Writing - Review & Editing, Validation.

ACKNOWLEDGEMENTS

The authors acknowledge the computational facilities and resources available at Sanskaram University, Patauda, Jhajjar, Haryana, India.

LIST OF ABBREVIATIONS

Abbreviation	=	Full Form
MNPs	=	Micro- and Nanoplastics
MPs	=	Microplastics
NPs	=	Nanoplastics
DEHP	=	Di(2-ethylhexyl) phthalate
DBP	=	Di-n-butyl phthalate
DIBP	=	Diisobutyl phthalate
BBP	=	Benzyl butyl phthalate
DCP	=	Dicyclohexyl phthalate
TGF-β	=	Transforming growth factor-beta
SMAD	=	Sma and Mad homolog
TGFβRI	=	TGF-β Receptor I
TGFβRII	=	TGF-β Receptor II
MH2	=	Mad Homology 2 domain
ECM	=	Extracellular Matrix
NF-κB	=	Nuclear factor kappa B
PI3K/AKT/mTOR	=	Phosphoinositide 3-kinase/AKT/mechanistic target of rapamycin

MAPK = Mitogen-activated protein kinase

AhR = Aryl hydrocarbon receptor

EMT = Epithelial-Mesenchymal Transition

TSCA = Toxic Substances Control Act

US EPA = United States Environmental Protection Agency

IARC = International Agency for Research on Cancer

PDB = Protein Data Bank

ADT = AutoDock Tools

LGA = Lamarckian Genetic Algorithm

DSV = Discovery Studio Visualizer

ΔG = Gibbs free energy of binding

NB = No Binding

REFERENCES

[1] Kumar N, Singh JK, Mandal M, Yadav N, Tyagi D. The Hidden Poison: How Microplastics and Nanoplastics Threaten the Health of Aquatic Organisms Across Ecosystems. In: Microplastics and Nanoplastics in Aquatic Environments. London: IntechOpen Limited 2026. https://doi.org/10.5772/intechopen.1013156

[2] Irfan H, Irfan H, Khan MA, Inanc O, Al Hasibuzzaman M. Microplastics and nanoplastics: emerging threats to cardiovascular health–a comprehensive review. Ann Med Surg 2025; 87(1): 209-16. https://doi.org/10.1097/MS9.0000000000002831

[3] Kumar N, Lamba M, Pachar AK, Yadav S, Acharya A. Microplastics–a growing concern as carcinogens in cancer etiology: emphasis on biochemical and molecular mechanisms. Cell Biochem Biophys 2024; 82(4): 3109-21. https://doi.org/10.1007/s12013-024-01436-0

[4] Roslan NS, Lee YY, Ibrahim YS, Anuar ST, Yusof KMKK, Lai LA, *et al*. Detection of microplastics in human tissues and organs: A scoping review. J Glob Health 2024; 14: 04179. https://doi.org/10.7189/jogh.14.04179

[5] Li Y, Yang H, He W, Li Y. Human endocrine-disrupting effects of phthalate esters through adverse outcome pathways: A comprehensive mechanism analysis. Int J Mol Sci 2023; 24(17): 13548. https://doi.org/10.3390/ijms241713548

[6] Kannan K, Vimalkumar K. A review of human exposure to microplastics and insights into microplastics as obesogens. Front Endocrinol 2021; 12: 724989. https://doi.org/10.3389/fendo.2021.724989

[7] Tang KHD. Counteracting the harms of microplastics on humans: An overview from the perspective of exposure. Microplastics 2025; 4(3): 47. https://doi.org/10.3390/microplastics4030047

[8] Nihart AJ, Garcia MA, El Hayek E, Liu R, Olewine M, Kingston JD, *et al*. Bioaccumulation of microplastics in decedent human brains. Nat Med 2025; 31(4): 1114-9. https://doi.org/10.1038/s41591-024-03453-1

[9] Zhang R, Zhou Y, Zhao X, Chen Q, Li X, Chen Y, *et al*. Identification and analysis of microplastics in main organs of human fetus. Ecotoxicol Environ Saf 2026; 314: 120078. https://doi.org/10.1016/j.ecoenv.2026.120078

[10] Marfella R, Prattichizzo F, Sardu C, Fulgenzi G, Graciotti L, Spadoni T, *et al*. Microplastics and nanoplastics in atheromas and cardiovascular events. N Engl J Med 2024; 390(10): 900-10. https://doi.org/10.1056/NEJMoa2309822

[11] Liu Y, Wu NN, Xu R, Li ZH, Xu XR, Liu S. Phthalates released from microplastics can't be ignored: Sources, fate, ecological risks, and human exposure risks. TrAC Trends Anal Chem 2024; 179: 117870. https://doi.org/10.1016/j.trac.2024.117870

[12] Rowdhwal SSS, Chen J. Toxic effects of di-2-ethylhexyl phthalate: an overview. Biomed Res Int 2018 2018(1): 1750368. https://doi.org/10.1155/2018/1750368

[13] US EPA. America's Children and the Environment. 3rd ed. Washington, DC: U.S. Environmental Protection Agency 2013.

[14] Zota AR, Calafat AM, Woodruff TJ. Temporal trends in phthalate exposures: findings from the National Health and Nutrition Examination Survey. Environ Health Perspect 2014; 122(3): 235-41. https://doi.org/10.1289/ehp.1306681

[15] US EPA. Designation of High-Priority Substances and Explanation of Designation for Substances Identified in TSCA Section 6(b)(1)(B)(i): Final Rule. Washington, DC: U.S. Government Publishing Office 2019.

[16] Payne-Sturges D, De Saram S, Cory-Slechta DA. Cumulative risk evaluation of phthalates under TSCA. Environ Sci Technol 2023; 57(16): 6403-14. https://doi.org/10.1021/acs.est.2c08364

[17] Pillo G, Aldrovandi F, Mescoli A, Maffei G, Mascolo MG, Vaccari M, *et al*. An insight into carcinogenic activity and molecular mechanisms of Bis (2-ethylhexyl) phthalate. Front Toxicol 2024; 6: 1389160. https://doi.org/10.3389/ftox.2024.1389160

[18] Tiburcio D, Parsell M, Shapiro H, Adolphe S, Naranjo O, George S, *et al*. Endocrine disruption to metastasis: How phthalates promote breast carcinogenesis. Ecotoxicol Environ Saf 2025; 303: 118874. https://doi.org/10.1016/j.ecoenv.2025.118874

[19] Chen J, Pang H, Wang J, Guo J, Huang T, Zhou H. Multi-scale systems toxicology defines a KLF5-centered adverse outcome pathway linking DEHP exposure to pancreatic cancer progression and signaling programs relevant to therapy tolerance. Front Cell Dev Biol 2026; 14: 1769023. https://doi.org/10.3389/fcell.2026.1769023

[20] Amir S, Shah STA, Mamoulakis C, Docea AO, Kalantzi OI, Zachariou A, *et al*. Endocrine disruptors acting on estrogen and androgen pathways cause reproductive disorders through multiple mechanisms: a review. Int J Environ Res Public Health 2021; 18(4): 1464. https://doi.org/10.3390/ijerph18041464

[21] Hyman S, Acevedo J, Giannarelli C, Trasande L. Phthalate exposure from plastics and cardiovascular disease: global estimates of attributable mortality and years life lost. EBioMedicine 2025; 117: 1-15. https://doi.org/10.1016/j.ebiom.2025.105730

[22] Wang L, Qin Y, Fan W. Exploring the toxicological impact of DEHP exposure on colorectal cancer through network toxicology, machine learning and bioinformatics analysis. BMC Pharmacol Toxicol 2025. https://doi.org/10.1186/s40360-025-01065-0

[23] Wang Z, Wang Y. Mechanism exploration of di (2-ethylhexyl) phthalate (DEHP)-induced breast cancer via network toxicology and molecular docking analysis. Sci Rep 2025; 15(1): 27257. https://doi.org/10.1038/s41598-025-13201-1

[24] Yin Z, Jin X, Mao C, Kang L, Gong C, Feng S, *et al*. Analysis of toxicity and mechanisms of DEHP in prostate cancer with network toxicology and molecular docking strategy. Int J Surg 2025; 111(1): 1454-7. https://doi.org/10.1097/JS9.0000000000001857

[25] Ran B, Wang X, Liu B, Ye J, Liu L, Yin Z, *et al*. Toxicity and mechanistic analysis of di (2-ethylhexyl) phthalate in renal cell carcinoma progression: a systematic study with network toxicology and molecular docking strategies. Discov Oncol 2025; 16(1): 1853. https://doi.org/10.1007/s12672-025-03543-7

[26] Chen Z, Wang C, Li Y, Xiao X, Zhao H, He B, *et al*. Mechanistic insights into DEHP-induced progression of non-small cell lung cancer based on network toxicology and molecular docking. Sci Rep 2025. Article in Press. https://doi.org/10.1038/s41598-025-28356-0

[27] Zhang Y, Wang Q. Network toxicological insights into DEHP exposure and thyroid cancer development and progression. Front Oncol 2025; 15: 1617202. https://doi.org/10.3389/fonc.2025.1617202

[28] Zhang J, Zhang W, Zhang L, He J, Dong Y, Yuan J. Investigating the mechanism of phthalates in breast cancer using molecular docking and network toxicology. Toxicol Mech Methods 2025; 35(9): 1547-65. https://doi.org/10.1080/15376516.2025.2553099

[29] Yang X, Bai Z, Yan X, Zhou Y, Zhong C, Wu J. Computer-aided molecular design meets network toxicology and molecular docking: a joint strategy to explore common molecular mechanisms of phthalates on human breast cancer and structure-activity relationship. Int J Mol Sci 2025; 26(20): 9878. https://doi.org/10.3390/ijms26209878

[30] Wang Z, Ma L, Sun Z, Lv H, Ma R, Ding M, *et al*. Elucidating key targets and mechanisms of diethyl phthalate-induced colorectal cancer through network toxicology and molecular docking. PLoS One 2026; 21(2): e0343038. https://doi.org/10.1371/journal.pone.0343038

[31] Kumar N, Pachar AK, Singh JK, Mandal M, Lamba M, Yadav S, *et al*. Investigating the hypothesis role of the hidden poison microplastics in lymphoma development. Discov Environ 2025; 3(1): 73. https://doi.org/10.1007/s44274-025-00224-8

[32] Morris GM, Huey R, Lindstrom W, Sanner MF, Belew RK, Goodsell DS, *et al*. AutoDock4 and AutoDockTools4: Automated docking with selective receptor flexibility. J Comput Chem 2009; 30(16): 2785-91. https://doi.org/10.1002/jcc.21256

[33] Trott O, Olson AJ. AutoDock Vina: improving the speed and accuracy of docking with a new scoring function, efficient optimization, and multithreading. J Comput Chem 2010; 31(2): 455-61. https://doi.org/10.1002/jcc.21334

[34] Isgrò C, Sardanelli AM, Palese LL. Systematic search for SARS-CoV-2 main protease inhibitors for drug repurposing: Ethacrynic acid as a potential drug. Viruses 2021; 13(1): 106. https://doi.org/10.3390/v13010106

[35] Patel CN, Kumar SP, Pandya HA, Rawal RM. Identification of potential inhibitors of coronavirus hemagglutinin-esterase using molecular docking, molecular dynamics simulation and binding free energy calculation. Mol Divers 2021; 25(1): 421-33. https://doi.org/10.1007/s11030-020-10135-w

[36] Massagué J, Sheppard D. TGF-β signaling in health and disease. Cell 2023; 186(19): 4007-37. https://doi.org/10.1016/j.cell.2023.07.036

[37] Giarratana AO, Prendergast CM, Salvatore MM, Capaccione KM. TGF-β signaling: critical nexus of fibrogenesis and cancer. J Transl Med 2024; 22(1): 594. https://doi.org/10.1186/s12967-024-05411-4

[38] Runa F, Ortiz-Soto G, de Barros NR, Kelber JA. Targeting SMAD-dependent signaling: considerations in epithelial and mesenchymal solid tumors. Pharmaceuticals 2024; 17(3): 326. https://doi.org/10.3390/ph17030326

[39] Giovanoulis G, Bui T, Xu F, Papadopoulou E, Padilla-Sanchez JA, Covaci A, *et al*. Multi-pathway human exposure assessment of phthalate esters and DINCH. Environ Int 2018; 112: 115-26. https://doi.org/10.1016/j.envint.2017.12.016

[40] Kim HG, Lim YS, Hwang S, Kim HY, Moon Y, Song YJ, *et al*. Di-(2-ethylhexyl) phthalate triggers proliferation, migration, stemness, and epithelial–mesenchymal transition in human endometrial and endometriotic epithelial cells via the transforming growth factor-β/SMAD signaling pathway. Int J Mol Sci 2022; 23(7): 3938. https://doi.org/10.3390/ijms23073938

[41] Liu X, He DW, Zhang DY, Lin T, Wei GH. Di (2-ethylhexyl) phthalate (DEHP) increases transforming growth factor-β1 expression in fetal mouse genital tubercles. J Toxicol Environ Health A 2008; 71(19): 1289-94. https://doi.org/10.1080/15287390802114915

[42] Zhou Y, Huang F, Liu Y, Li D, Zhou Y, Shen L, *et al*. TGF-β1 relieves epithelial–mesenchymal transition reduction in hypospadias induced by DEHP in rats. Pediatr Res 2020; 87(4): 639-46. https://doi.org/10.1038/s41390-019-0622-2

[43] Hua S, Shi F, Xie Z, Wu L, Dai M, Zhang Y, *et al*. Di-n-butyl phthalate induces oversecretion of vascular endothelium-derived NAP-2 and promotes epithelial-mesenchymal transition of urothelial cells in newborn hypospadias rats. Ecotoxicol Environ Saf 2023; 256: 114892. https://doi.org/10.1016/j.ecoenv.2023.114892

[44] Yost EE, Euling SY, Weaver JA, Beverly BE, Keshava N, Mudipalli A, *et al*. Hazards of diisobutyl phthalate (DIBP) exposure: a systematic review of animal toxicology studies. Environ Int 2019; 125: 579-94. https://doi.org/10.1016/j.envint.2018.09.038

[45] Shukla R, Mahmuda A, Laws MJ, Flaws JA, Bagchi MK, Wagoner Johnson AJ, *et al*. Chronic exposure of mice to phthalates enhances TGF beta signaling and promotes uterine fibrosis. Reprod Toxicol 2023; 122: 108491. https://doi.org/10.1016/j.reprotox.2023.108491

[46] Schettler T. Human exposure to phthalates via consumer products. Int J Androl 2006; 29(1): 134-9. https://doi.org/10.1111/j.1365-2605.2005.00567.x

[47] Wang W, Liu Z, Zhang Y, Wang L, Meng D, Li X, *et al*. Benzyl butyl phthalate (BBP) induces lung injury and fibrosis through neutrophil extracellular traps. Environ Pollut 2022; 309: 119743. https://doi.org/10.1016/j.envpol.2022.119743

[48] Wang YC, Tsai CF, Chuang HL, Chang YC, Chen HS, Lee JN, *et al*. Benzyl butyl phthalate promotes breast cancer stem cell expansion via SPHK1/S1P/S1PR3 signaling. Oncotarget 2016; 7(20): 29563-75. https://doi.org/10.18632/oncotarget.9007

[49] Charrette BP, Boerneke MA, Hermann T. Ligand optimization by improving shape complementarity at a hepatitis C virus RNA target. ACS Chem Biol 2016; 11(12): 3263-7. https://doi.org/10.1021/acschembio.6b00687

[50] Romines KR, Watenpaugh KD, Tomich PK, Howe WJ, Morris JK, Lovasz KD, *et al*. Use of medium-sized cycloalkyl rings to enhance secondary binding: discovery of a new class of human immunodeficiency virus (HIV) protease inhibitors. J Med Chem 1995; 38(11): 1884-91. https://doi.org/10.1021/jm00011a008

[51] Peng D, Fu M, Wang M, Wei Y, Wei X. Targeting TGF-β signal transduction for fibrosis and cancer therapy. Mol Cancer 2022; 21(1): 104. https://doi.org/10.1186/s12943-022-01569-x

[52] Ganesh H, Moran J, Roy S, Mathew J, Ackah-Blay J, Costello E, *et al*. Impact of persistent endocrine-disrupting chemicals on human nuclear receptors: insights from in silico and experimental characterization. Int J Mol Sci 2025; 26(7): 2879. https://doi.org/10.3390/ijms26072879

[53] US EPA. Risk Evaluation for Dicyclohexyl Phthalate (DCHP). Washington, DC: U.S. Environmental Protection Agency, Office of Chemical Safety and Pollution Prevention 2025.

[54] Requena P, Pérez-Díaz C, Mustieles V, Peinado FM, León J, Pérez-Carrascosa FM, *et al*. Associations of circulating levels of phthalate metabolites with cytokines and acute phase reactants in a Spanish human cohort. Environ Res 2023; 216: 114470. https://doi.org/10.1016/j.envres.2022.114470

[55] Ren LL, Li XJ, Duan TT, Li ZH, Yang JZ, Zhang YM, *et al*. Transforming growth factor-β signaling: from tissue fibrosis to therapeutic opportunities. Chem Biol Interact 2023; 369: 110289. https://doi.org/10.1016/j.cbi.2022.110289

[56] Sheikh KA, Amjad M, Irfan MT, Anjum S, Majeed T, Riaz MU, *et al*. Exploring TGF-β signaling in cancer progression: prospects and therapeutic strategies. OncoTargets Ther 2025: 233-62. https://doi.org/10.2147/OTT.S493643

[57] Deng Z, Fan T, Xiao C, Tian H, Zheng Y, Li C, *et al*. TGF-β signaling in health, disease and therapeutics. Signal Transduct Target Ther 2024; 9(1): 61. https://doi.org/10.1038/s41392-024-01764-w

[58] Parichatikanond W, Luangmonkong T, Mangmool S, Kurose H. Therapeutic targets for the treatment of cardiac fibrosis and cancer: focusing on TGF-β signaling. Front Cardiovasc Med 2020; 7: 34. https://doi.org/10.3389/fcvm.2020.00034

[59] Ogunjimi AA, Zeqiraj E, Ceccarelli DF, Sicheri F, Wrana JL, David L. Structural basis for specificity of TGFβ family receptor small molecule inhibitors. Cell Signal 2012; 24(2): 476-83. https://doi.org/10.1016/j.cellsig.2011.09.027

[60] Tebben AJ, Ruzanov M, Gao M, Xie D, Kiefer SE, Yan C, *et al*. Crystal structures of apo and inhibitor-bound TGFβR2 kinase domain: insights into TGFβR isoform selectivity. Acta Crystallogr D Biol Crystallogr 2016; 72(5): 658-74. https://doi.org/10.1107/S2059798316003624

[61] Wu JW, Hu M, Chai J, Seoane J, Huse M, Li C, *et al*. Crystal structure of a phosphorylated Smad2: recognition of phosphoserine by the MH2 domain and insights on Smad function in TGF-β signaling. Mol Cell 2001; 8(6): 1277-89. https://doi.org/10.1016/S1097-2765(01)00421-X

[62] Chacko BM, Qin BY, Tiwari A, Shi G, Lam S, Hayward LJ, *et al*. Structural basis of heteromeric smad protein assembly in TGF-β signaling. Mol Cell 2004; 15(5): 813-23. https://doi.org/10.1016/j.molcel.2004.07.016

Received on 30-07-2026 Accepted on 25-08-2026 Published on 08-09-2026

https://doi.org/10.30683/1929-2279.2026.15.24